JCTC Journal of Chemical Theory and Computation

Article

pubs.acs.org/JCTC

On the Origin of $^{35/37}$Cl Isotope Effects on ^{195}Pt NMR Chemical Shifts. A Density Functional Study

John C. Davis,[†,‡] Michael Bühl,*[,†] and Klaus R. Koch*[,‡]

[†]School of Chemistry, University of St. Andrews, North Haugh, St. Andrews, Fife KY16 9ST, U.K.

[‡]Department of Chemistry and Polymer Science, University of Stellenbosch, P Bag X1, Matieland, 7602, South Africa

Supporting Information

ABSTRACT: Zero-point vibrationally averaged (r_g^0) structures were computed at the PBE0/SDD/6-31G* level for $[Pt^{35}Cl_6]^{2-}$ and $[Pt^{37}Cl_6]^{2-}$, for the $[Pt^{35}Cl_n{}^{37}Cl_{5-n}(H_2O)]^-$ (n = 0−5), *cis*-$Pt^{35}Cl_n{}^{37}Cl_{(4-n)}(H_2O)_2$ (n = 0−4), and *fac*-$[Pt^{35}Cl_n{}^{37}Cl_{(3-n)}(H_2O)_3]^+$ (n = 0−3) isotopologues and isotopomers. Magnetic ^{195}Pt shielding constants, computed at the ZORA-SO/PW91/QZ4P/TZ2P level, were used to evaluate the corresponding $^{35/37}$Cl isotope shifts in the experimental ^{195}Pt NMR spectra. While the observed effects are reproduced reasonably well computationally in terms of qualitative trends and the overall order of magnitude (ca. 1 ppm), quantitative agreement with experiment is not yet achieved. Only small changes in Pt−Cl and Pt−O bond lengths upon isotopic substitution, on the order of femtometers, are necessary to produce the observed isotope shifts.

1. INTRODUCTION

Owing to their huge chemical shift ranges, transition metal nuclei can be highly sensitive NMR probes. Unfortunately, many of these nuclei have large quadrupole moments, which limits the applicability and usefulness of this spectroscopic technique for analytical purposes. The spin 1/2 nucleus ^{195}Pt is a notable exception. ^{195}Pt NMR spectroscopy has long been used to characterize diamagnetic Pt complexes and, fueled by the additional interest in Pt-containing drugs, an immense body of Pt NMR data is available.[1] The ^{195}Pt nucleus can be so sensitive to its environment that, for instance, rather subtle isotope effects can be detected. Already three decades ago, Sadler et al. demonstrated that at higher magnetic fields (9.4 T) the ^{35}Cl/^{37}Cl isotope shifts can be resolved for the $[Pt^{35}Cl_n{}^{37}Cl_{6-n}]^{2-}$ (n = 0−6) complex in aqueous solution, with a shielding of ca. 0.167 ppm per incorporated ^{37}Cl isotope.[2] Preetz et al. reported similar isotope shifts (ca. 0.18 ppm) for a subset of these isotopologues (n = 2−6).[3] The elegant fundamental work on the origin of the isotope shift and temperature dependence of the NMR shielding in MX_6 type molecules by Jameson et al.[4] demonstrates a direct proportionality of an isotope shift to a $(m' - m)/m'$ factor (where m and m' are the atomic masses of the isotopes of X bonded to M), which in turn depends on the mean M−X bond displacement at a given temperature, r_g, as confirmed by experimental measurements.

Modern high-resolution spectrometers have taken the applicability of ^{195}Pt NMR even further. In speciation studies of mixed chloro/aquo platinum(IV) complexes in acidic solution not only the signals for the expected ^{35}Cl/^{37}Cl isotopologues have been observed, but some peaks could be resolved into characteristic multiplets.[5] The latter were assigned to complexes termed isotopomers, which contain the same number of each Cl isotope, but distributed over different nonequivalent sites. Thus, isotope shifts observed in ^{195}Pt NMR resonances afford "fingerprints" of isotopic stereoisomers by their unique isotopologue and isotopomer distributions (see Figure S1 in the Supporting Information for some representative spectra).

Assignment of individual resonances to specific isotopologues and isotopomers in the experimental ^{195}Pt NMR spectra was achieved through the intensity ratios of the individual peaks, assuming statistical distribution of the different isotopes involved. It would be desirable to be able to compute such isotope shifts from first principles, in order to provide a solid theoretical framework for the empirical observations, and to have a means of assignment in cases where the statistical distribution would be ambiguous. Quantum-chemical computation of transition metal chemical shifts is a stronghold of density-functional theory (DFT),[6] and the advent of relativistic methods such as the zero-order regular approximation (ZORA) have made ^{195}Pt NMR parameters amenable to computational study.[7]

Most of these calculations employ static equilibrium structures, which are independent of atomic masses. Using zero-point vibrationally averaged structures, isotope effects on ^{59}Co chemical shifts have been reproduced and rationalized computationally.[8] In a cobaloxime[8a] and the hexamine cobalt(III) complex,[8b] the observed ^{1}H/^{2}H shifts on the order of ca. 50−100 ppm could be traced back to small changes in the Co−N bonds, on the order of 0.001−0.006 Å, upon isotopic substitution. Because of their much smaller magnitude, typically 1 ppm or less,[5] the above-mentioned isotope effects on ^{195}Pt shifts pose a much bigger challenge to theory. We now report a density functional theory (DFT) study of the $^{35/37}$Cl induced isotope shifts in the ^{195}Pt NMR spectra of some prototypical Pt(IV) chlorido/aqua complexes, $[PtCl_{6-n}(H_2O)_n]^{n-2}$ (n = 0−3). As it turns out, the order of magnitude of the observed isotope shifts can be reproduced by

Received: February 6, 2012
Published: February 28, 2012

the computed zero-point corrections, but quantitative accuracy is not reached yet.

2. COMPUTATIONAL DETAILS

Geometries were fully optimized at the PBE0/ECP1 level, i.e., employing the hybrid variant of the PBE functional,[9] the Stuttgart–Dresden relativistic effective core potential (SDD ECP) along with its [6s5p3d] valence basis on Pt,[10] and 6-31G* basis[11] elsewhere. This combination of functional and basis sets has performed very well for the description of bond distances between third-row transition metals and their ligands.[12] Preliminary performance tests of selected other functional/ECP combinations are summarized in Table S1 and Figure S2 in the Supporting Information. Unless otherwise noted, tight optimization criteria and a fine integration grid were employed (opt=tight, grid=finegrid options in Gaussian). Selected complexes were reoptimized using the same ECP and basis sets in conjunction with the LDA,[13] B3LYP,[14] B3PW91,[14a,15] and M06 functionals, as well as (at the PBE0/ECP1 level) with the CPCM method,[16] the equivalent of the conductor-like screening model (COSMO), as implemented in Gaussian 09, together with the parameters of water.

Effective geometries, r_g^0 at 0 K, were constructed in a perturbational approach from the equilibrium geometries r_e, the (mass-dependent) harmonic frequencies ω_e, and the cubic force field $V^{(3)}$ (see refs 17 and 18 for details):

$$r_{g,j}{}^0 = r_{e,j} + \Delta r_{g,j}{}^0 = r_{e,j} - \frac{1}{4\omega_{e,j}{}^2}\sum_m \frac{V^{(3)}_{e,jmm}}{\omega_{e,m}} \quad (1)$$

These calculations were performed using the Gaussian09 suite of programs.[19]

For r_e and r_g^0 geometries of each isotopic substitution, ^{195}Pt shielding tensors were computed at the relativistic spin–orbit ZORA level, using the GGA PW91[15] functional, together with an all-electron quadruple-ζ plus polarization function (QZ4P) basis set on Pt and polarized valence triple-ζ basis sets (TZP) on Cl and H_2O.[20] The integration precision parameter was set to 10.0. These calculations employed the ADF2010.02 program.[21] The particular flavor of GGA functionals has only little effect on ^{195}Pt chemical shifts;[22] we used PW91 because it had performed well in a previous study of mixed $[PtX_6]^{2-}$ halides (X = Cl, Br).[7e]

3. RESULTS AND DISCUSSION

3.1. Numerical Stability. From the observed isotope shift between $[Pt^{35}Cl_6]^{2-}$ and $[Pt^{37}Cl_6]^{2-}$, $\Delta\delta(^{195}Pt) \approx 1$ ppm,[2,3] and the computed shielding/bond-length derivative of $[PtCl_6]^{2-}$, $\partial\sigma^{Pt}/\partial r_{PtCl} = -18\,300$ ppm/Å (ZORA/PW91/TZP/COSMO level),[7e] it can be estimated that the changes in bond lengths brought about by the isotopic substitution should be on the order of ca. 6×10^{-5} Å. Such small effects place quite stringent demands not only on the accuracy of the methods to be applied, but also on the numerical stability of the zero-point corrections evaluated through eq 1. Because the cubic force field $V^{(3)}$ is obtained through numerical differentiation of analytical second derivatives, it must be made sure that the numerical noise introduced this way is not larger than the actual effects under scrutiny. Besides the step size involved in the creation of the displaced structures, the most important parameter is the size of the grid involved in the numerical integration of the exchange-correlation potential for energies and second derivatives (in the coupled perturbed Kohn–Sham equations). We have used pristine *cis*-$PtCl_4(H_2O)_2$ (**2**, Figure 1) as test molecule, gauging convergence of the results from the

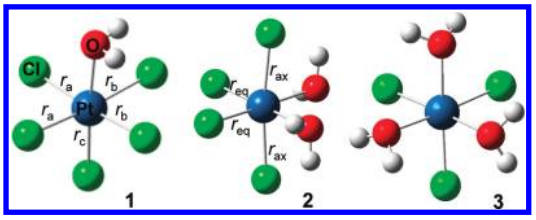

Figure 1. Optimized structures of $[PtCl_5(H_2O)]^-$ (**1**, left), *cis*-$PtCl_4(H_2O)_2$ (**2**, middle), and *fac*-$[PtCl_3(H_2O)_3]^+$ (**3**, right).

computed effects of vibrational averaging on the Pt–Cl distances in the all-^{35}Cl and all-^{37}Cl isotopomers (Tables 1 and 2).

Table 1 summarizes the equilibrium distances r_e and their changes $\Delta r_g{}^0$ upon inclusion of the zero-point vibrational corrections as a function of grid and step sizes in the numerical integration and differentiation steps involved. Ideally the results should converge smoothly with increasing grids and decreasing step size, i.e., going down and to the right in Table 1. The default setting in Gaussian is to use fine and coarse grids in the evaluation of energies and the solution of the coupled perturbed Kohn–Sham (CPKS) equations, respectively (C/A combination in the labeling of Table 1), together with a step size of 0.01 au. Even with the slightly better fine/SG1 grid combination (C/B) the results are not sufficiently converged, however: further increase in grid quality (i.e., going from C/B to D/C) affects the equilibrium distances and the vibrational corrections by up to 10^{-4} Å, that is, above the desired accuracy. Further improvement of the grid (e.g., from D/C to E/D) results in only minor changes, 2×10^{-5} Å or less (see Figure S3 in the Supporting Information for a graphical representation). Reassuringly, the vibrational corrections are only faintly sensitive to the step size (compare Δr as a function of d in Table 1), in contrast to some first-row transition metal complexes, where this parameter proved to be important for the numerical stability.[24] We note in passing that the overall magnitude of the zero-point corrections for the Pt–Cl bonds, on the order of ca. 0.2–0.3 Å, is very similar to that obtained for other 5d-metal chlorides.[12]

The same test calculations were carried out for the *cis*-$Pt^{37}Cl_4(H_2O)_2$ isotopologue. The resulting differences in the vibrational corrections between the ^{35}Cl and ^{37}Cl complexes (i.e., between the corresponding r_g^0 values) are summarized in Table 2 (note that these $\Delta\Delta r$ values are now reported in units of 10^{-5} Å; for the actual distances in the ^{37}Cl isotopomer see Table S2 in the Supporting Information). As expected from the effect of anharmonicity, Pt–^{35}Cl bonds are longer than Pt–^{37}Cl bonds. Even though these isotope effects are now relative trends rather than absolute values, little error compensation is to be expected, because we are assessing numerical precision, not accuracy. Nonetheless, the same convergence pattern as for the vibrational corrections in Table 1 is apparent, and the largest change between any $\Delta\Delta^{35/37}r$ value on going from the D/C to the E/D grids is 2.8×10^{-5} Å. Taking the computational expense into account (last column in Table 1), the ultrafine/fine grid combination (D/C) and the default step size of 0.01 au appeared to be the best compromise between precision and speed and was adopted for all further calculations.

dx.doi.org/10.1021/ct300105q | J. Chem. Theory Comput. 2012, 8, 1344–1350

Table 1. Equilibrium Bond Lengths (r_e) and Differences between Equilibrium and Effective Bond Lengths at 0 K (Δr_{eq} and Δr_{ax}) in *cis*-$Pt^{35}Cl_4(H_2O)_2$ [Å], Obtained with Different Grids and Step Lengths d [au] in the Numerical Integration and Differentiation, Respectively[a]

	r_e[c]		d = 0.1		d = 0.01		d = 0.001		
grids[b]	$r_{e,eq}$	$r_{e,ax}$	$\Delta r_{g,eq}{}^0$	$\Delta r_{g,ax}{}^0$	$\Delta r_{g,eq}{}^0$	$\Delta r_{g,ax}{}^0$	$\Delta r_{g,eq}{}^0$	$\Delta r_{g,ax}{}^0$	CPU hours[d]
B/A	2.272 205(0)	2.336 298(4)	0.002 444	0.005 812	0.002 356	0.005 873	0.002 355	0.005 871	10.5
C/B	2.275 561(0)	2.337 360(2)	0.002 313	0.003 060	0.002 251	0.003 028	0.002 250	0.003 026	11.5
D/C	2.275 548(0)	2.337 465(1)	0.002 418	0.003 111	0.002 379	0.003 094	0.002 378	0.003 082	27.0
E/D	2.275 536(1)	2.337 448(1)	0.002 437	0.003 109	0.002 401	0.003 095	0.002 401	0.003 092	63.0

[a]PBE0/SDD/6-31G* level. [b]Numerical integration grids involved in energy/CPKS evaluations, labeled A (35, 110), B (50, 194), C (75, 302), D (99, 590), and E (99, 770) (numbers in parentheses are radial and angular grid points, respectively). [c]Average value of the two axial r_{ax} and two equatorial bonds r_{eq} (in parentheses, standard deviation in units of the last digit; cf. ref 23). [d]Approximate runtime on eight CPUs of a local Opteron PC cluster.

Table 2. Differences $\Delta\Delta^{35/37}r$ between Effective Pt−Cl Distances in *cis*-$Pt^{35}Cl_4(H_2O)_2$ and *cis*-$Pt^{37}Cl_4(H_2O)_2$ in Units of 10^{-5} Å, Obtained with Different Grids and Step Lengths d [a.u] in the Numerical Integration and Differentiation, Respectively[a]

	d = 0.1		d = 0.01		d = 0.001	
grids[b]	$\Delta\Delta^{35/37}r_{eq}$	$\Delta\Delta^{35/37}r_{ax}$	$\Delta\Delta^{35/37}r_{eq}$	$\Delta\Delta^{35/37}r_{ax}$	$\Delta\Delta^{35/37}r_{eq}$	$\Delta\Delta^{35/37}r_{ax}$
B/A	26.8	9.4	28.7	8.2	28.7	8.2
C/B	9.1	9.5	8.7	9.0	8.7	9.1
D/C	9.9	14.5	10.0	14.5	9.9	13.7
E/D	10.3	11.8	10.3	11.7	10.3	11.9

[a]PBE0/SDD/6-31G* level. [b]Numerical integration grids involved in energy/CPKS evaluations, labeled A (35, 110), B (50, 194), C (75, 302), D (99, 590), and E (99, 770) (numbers in parentheses are radial and angular grid points, respectively).

3.2. Isotope Shifts. Subsequently, all possible $^{35/37}Cl$ isotopomers were calculated in the gas phase for a representative set of mixed Pt(VI) chloro/aquo complexes (**1**−**3**, see Figure 1), namely $[Pt^{35}Cl_n{}^{37}Cl_{5-n}(H_2O)]^-$ (n = 0−5), *cis*-$Pt^{35}Cl_n{}^{37}Cl_{(4-n)}(H_2O)_2$ (n = 0−4), and *fac*-$[Pt^{35}Cl_n{}^{37}Cl_{(3-n)}(H_2O)_3]^+$ (n = 0−3, see Figure 2). The resulting vibrationally averaged structures were used as inputs for relativistic calculations of the isotropic magnetic shielding constants at the ZORA-SO/PW91/QZ4P/TZ2P level. To compare with experiment, isotope shifts $\Delta\delta$ were calculated relative to the corresponding all-^{35}Cl isotopologue set to δ = 0.

Because the water molecules coordinate in a bent, "sp^3" mode, the symmetry of the isolated complexes in the gas phase is lower than that apparent on the NMR time scale, i.e., C_s instead of C_{4v} for **1**, C_2 instead of C_{2v} for **2**, and C_3 instead of C_{3v} for **3**. While this does not affect the number of possible isotopomers for **2** and **3**, for **1** there are many more static structures than experimentally resolved signals. However, many of the static structures can be interconverted through simple water rotation about the Pt−O bond or inversion at O, processes that are expected to occur very rapidly on the NMR time scale. It is thus reasonable to assume that those isotopomers of **1** that are grouped together in Figure 2 will only show a single NMR signal, and their computed shielding constants were averaged accordingly (arithmetically, because the isotopomers should be essentially degenerate energetically). The resulting shielding constants and the corresponding experimental isotope shifts are collected in Table S3 in the Supporting Information and, after conversion of the computed shieldings into relative shifts, plotted against each other in Figure 3. The sign of the experimental isotope shifts has been reversed, so they appear in the same sequence as in a conventional NMR spectrum.

Despite some scatter, the overall observed trends are reasonably well reproduced by our computational protocol. It is particularly gratifying that the overall order of magnitude of the isotope shifts, ca. 1 ppm, is rather well recovered computationally. Only the isotope shifts of the trichloride **3** appear to be overestimated by a factor of ca. 2. The sequence of individual, more closely spaced resonances (below ca. 0.2 ppm)

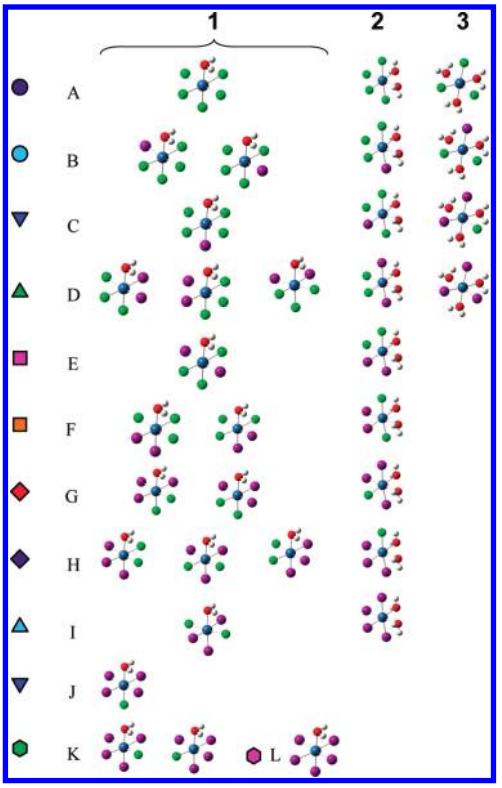

Figure 2. Isotopomers of $[PtCl_5(H_2O)]^-$ (**1**), *cis*-$PtCl_4(H_2O)_2$ (**2**), and *fac*-$[PtCl_3(H_2O)_3]^+$ (**3**), together with the labeling scheme adopted in the following figures. Color code: ^{35}Cl, green; ^{37}Cl, purple.

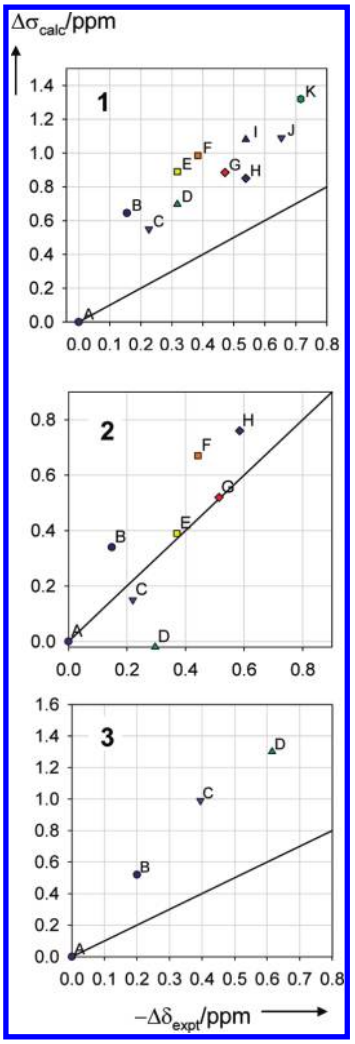

Figure 3. Calculated ^{195}Pt shielding differences vs negative experimental $^{35/37}$Cl isotope shifts of the isotopomers of **1**−**3** in Figure 2, including the ideal line with unity slope. Top: $[PtCl_5(H_2O)]^-$. Middle: *cis*-$PtCl_4(H_2O)_2$. Bottom: *fac*-$[PtCl_3(H_2O)_3]^+$.

is not always reproduced correctly, however. It is unclear at present whether these discrepancies are due to residual numerical errors in the computations, deficiencies of the overall model (e.g., the neglect of thermal effects beyond the zero-point corrections), or missing solvation (see below).

These minor inaccuracies notwithstanding, our results can be seen as the first theoretical rationalization of the observed isotope effects. ^{195}Pt NMR thus can effectively resolve chemical shift differences between complexes whose metal−ligand distances vary on the femtometer scale (cf. Table 2, 1 fm = 10^{-5} Å), a truly remarkable resolution. As commonly found for heavy-atom chemical shifts, it is the paramagnetic contribution to the shielding tensor, σ_{para}, that appears to dominate the overall observed ^{195}Pt shielding trends. The other contributions, namely the diamagnetic and spin−orbit terms, are rather insensitive to the isotopic substitution. This finding is illustrated in Table S4 and Figure S4 in the Supporting Information for the isotopomers of **2**.

How closely can the isotope shifts be linked to the variations in bond distances? To address this question, we used the shielding/bond-length derivatives $\partial\sigma_{Pt}/\partial r_{PtX}$ (X = O and Cl), together with the computed zero-point corrections for each bond length (Δr_g^0 in eq 1), in order to estimate effective shieldings according to

$$\sigma_{g,est}{}^0 = \sigma_e + \sum_{i=1}^{6} \Delta r_{g,i}{}^0 \frac{\partial\sigma_{Pt}}{\partial r_{PtX,i}} \quad (2)$$

These estimated shieldings can then be compared to the actual effective shieldings computed for the actual vibrationally averaged structure. For zero-point corrections to magnetic shieldings of first-row transition metals (spanning ca. 200 ppm), this breakdown into individual bond increments has worked very well.[25] Pt−Cl and Pt−O shielding/bond-length derivatives have been evaluated for **1**−**3** by rigid scans of the Pt−Cl and Pt−O bonds about their equilibrium values (see Figure S5 in the Supporting Information). The resulting $\partial\sigma_{Pt}/\partial r_{PtX}$ values are remarkably different for the different bonds, ranging from ca. −2100 to ca. −4200 ppm/Å for Pt−Cl bonds, and from ca. −1900 to ca. −3200 ppm/Å for Pt−O bonds (see Table S5 in the Supporting Information for the specific values). These $\partial\sigma_{Pt}/\partial r_{PtX,i}$ values were subsequently used to evaluate the increments to $\sigma_{g,est}{}^0$ from the $\Delta r_{g,i}{}^0$ values in **1**−**3** for each bond i (using the appropriate $\partial\sigma_{Pt}/\partial r_{PtX,i}$ value from Table S5 in the Supporting Information). Figure 4 shows the resulting

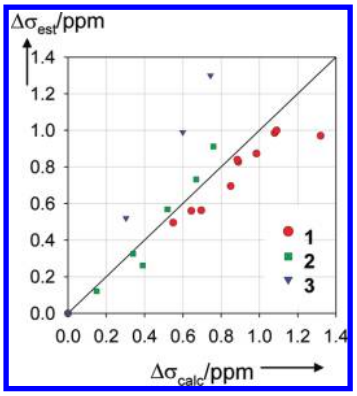

Figure 4. Shielding differences in $^{35/37}$Cl isotopomers of **1**−**3**, estimated from eq 2 vs actual computation from r_g^0 geometries, including the line with unity slope.

estimated $^{37/35}$Cl isotope effects on the ^{195}Pt shieldings of **1**−**3**, plotted vs the actual computed values (cf. Figure 3). Qualitative trends in the $\Delta\sigma$ values are described rather well by the increment method. Notwithstanding some scatter at the deshielded end (which is probably due to bond-angle or nonadditivity effects), this result substantiates our underlying model, namely that the bond-length changes due to zero-point vibrations is the dominant factor influencing the isotope shifts.

3.3. Solvation Effects. So far all computations have been performed for isolated complexes in the gas phase. However, the strength of metal−ligand bonds can depend noticeably on solvation, in particular for protic ligands such as water. In many computational studies of transition metal aquo complexes it has been found that the M−OH_2 distances can decrease appreciably on going from the gas phase into an aqueous solution.[26] In DFT-based molecular dynamics (MD) studies of uranyl complexes,[27] similar findings were recently interpreted in terms of cooperative polarization of the water ligands by the metal and the surrounding solvent molecules.[28] The increased dipole of the polarized water reinforces the metal−water bond, with possible indirect effects on the other metal−ligand bonds

in the complex (e.g., the Pt−Cl bonds trans to the water ligands).

To explore how our results would depend on the environment, we have attempted to include solvation effects into our model. Despite occasional shortcomings, simple polarizable continuum models (PCMs) can describe metal−ligand bond distances in solution reasonably well.[26,27] We thus attempted to evaluate isotope effects on the Pt aquo complexes immersed in such a continuum (see section 2). Zero-point corrections in a continuum have been shown to be beneficial for $\delta(^{59}\mathrm{Co})$ of ionic cobalt complexes in water, where mean absolute errors with respect to experiment are reduced by hundreds of ppm compared to simple PCM-optimized structures.[8b] As discussed in section 3.1, we are aiming at much smaller effects, where numerical stability can become an issue. In this context, PCM methods pose an additional problem during construction of the molecular cavity, which is built from interlocking spheres around the atoms. These spheres are discretized into triangular tesserae, which may lead to additional numerical uncertainties in the evaluation of $V^{(3)}$ in eq 1 via finite displacements. In principle, results should converge with increasing number of surface discretization points (see Figure S6 in the Supporting Information for selected three-dimensional plots of the latter), but in practice this becomes difficult because of the increasing CPU time and program limitations. In fact, the highest density of discretization points that could be used in conjunction with the vibrational averaging scheme in Gaussian 09, 86 points/Å^2, is not sufficient to converge even the equilibrium distances to the desired precision, much less the zero-point corrections to them (see Table S6 and Figure S7 in the Supporting Information). For *cis*-$\mathrm{Pt}^{35/37}\mathrm{Cl}_4(\mathrm{H_2O})_2$, increasing the number of discretization points or integration grids can affect the $\Delta\Delta^{35/37}r$ values by up to 9.4×10^{-5} Å (Table S6 in the Supporting Information), i.e., above the desired target precision (cf. section 3.1). If $^{35/37}$Cl isotope shifts are calculated for all isotopomers of **2** nonetheless, a seemingly reasonable correlation with experiment is obtained, but the computed span of shifts, 25 ppm, is more than 1 order of magnitude larger than observed (Figure S8 in the Supporting Information). Clearly, simple continuum models are not suitable with our protocol for such small isotope shifts.

Explicit inclusion of solvent molecules is preferred over simple PCMs, but already for a complete first solvation shell this is a formidable task requiring sampling over a dynamic ensemble. Detailed first-principles molecular dynamics (MD) studies of Pt(II) and Pt(IV) complexes in aqueous solution are available,[29,30] though apparently not for mixed aquo/chlorido species. The solvation shell around Pt−halide and related complexes and the impact on the Pt shielding have been studied in exquisite detail.[30,31] As a first step toward such a full description of solvation, we have optimized a microsolvated, partially hydrated cluster, namely $[\mathrm{PtCl_5(H_2O)}]^-\cdot 2\mathrm{H_2O}$. Placing the two extra water molecules such that they each accept an $\mathrm{OH\cdots OH_2}$ hydrogen bond from the coordinated water ligand, the minimum shown in the top of Figure 5 is obtained.

During optimization, the H-bonded water molecules orient themselves such that additional O−H···Cl interactions are formed. This ordered, closed network of H-bonds is not necessarily a good model for the situation in solution, where water molecules from the second hydration sphere tend to donate H-bonds to other solvent molecules from the bulk, rather than bend "backward" to the solute.[29] Nonetheless, the microsolvated cluster shows the onset of the expected reinforcement of the Pt−water bond in solution: On going from pristine **2** to $[\mathrm{PtCl_5(H_2O)}]^-\cdot 2\mathrm{H_2O}$, the equilibrium Pt−O bond distance decreases from 2.156 to 2.112 Å, similar to what is found in a continuum (e.g., 2.118 Å for **2**). At the same time, the zero-point correction for the Pt−^{16}O distance changes from Δr_g^0 = 0.011 Å (Table S7 in the Supporting Information) to 0.008 Å upon microsolvation, consistent with a stronger, stiffer bond.

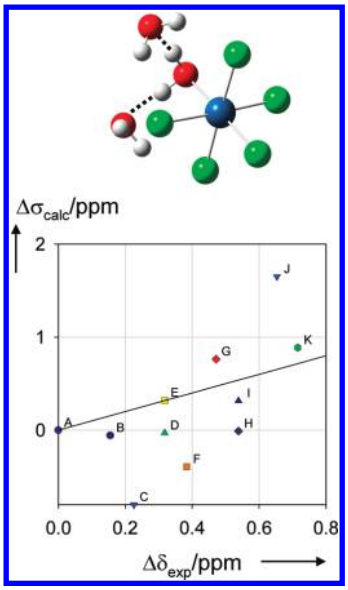

Figure 5. Calculated shielding differences vs negative experimental $^{35/37}$Cl isotope shifts of the isotopomers of $[\mathrm{PtCl_5(H_2O)}]^-\cdot 2\mathrm{H_2O}$ (shown at the top, labeling as in Figure 2), including the ideal line with unity slope.

How does this apparent change in the Pt−O stretching potential affect the isotope effects? The computed $^{35/37}$Cl shifts of all isotopomers are plotted against experiment in Figure 5. Comparing this plot to that of the pristine complex **2** (Figure 3) shows no visible improvement upon solvation. There are significant changes throughout, however, suggesting that solvent effects can indeed be very important.

Figure 5 seems to contain two rather distinct series of data points, where isotopomers C, F, H, I, and K form a linear correlation on their own (albeit with a much too large slope, ca. 4 instead of 1, and a significant offset from the ideal line). Interestingly, these are all the isotopomers that have a ^{37}Cl atom trans to the water ligand (Figure 2). Apparently, in our microsolvated complex the distinction between cis and trans chloride ligands is overestimated to a large extent, consistent with the fact that only the former interact with the extra water molecules, not the latter. Many more water molecules would have to be added, eventually necessitating a dynamical description (CPMD or QM/MM) and exceeding the scope of the present paper.

Besides such solvation effects, there could be other methodological shortcomings in our model that might compromise the accuracy of the results. As has been shown in a recent study of ^{199}Hg shieldings of small Hg(II) species, the ZORA-SO method does not accurately reproduce full four-component relativistic results and even the QZ4P basis set in ADF may not be fully saturated for this purpose.[32] Also, we are only evaluating shieldings at instantaneous r_g^0 (or r_{eff})

structures, ignoring effects from a possible curvature of the shielding hypersurface about this structure. While such effects tend to be small, they can be noticeable if high accuracy is sought.[33,34] Finally, only the zero-point motion is considered, ignoring contributions from thermal population of vibrationally excited states (the importance of which would increase with the atomic masses involved). We tacitly assume that all these effects, noticeable as they would be for the absolute shielding constants, are transferable enough between different molecules (or isotopomers) that they cancel to a large extent in the relative (i.e., isotope) shifts. Proper convergence of all these issues (i.e., computation of fully relativistic potential energy and shielding hypersurfaces at the basis-set limit) is, arguably, a formidable task. In light of the results discussed above in this section, we believe that proper inclusion of solvent effects may be rather more important.

4. CONCLUSION

In summary, we have presented calculations of magnetic shieldings at appropriate DFT levels for the isotopologues and isotopomers of Pt(IV) aqua/chlorido complexes. To this end, zero-point vibrationally averaged (r_g^0) structures were computed. The numerical stability of the underlying perturbational approach has been validated by employing different step sizes and grids of increasing precision in the numerical integration. Gas-phase geometries were calculated for $[Pt^{35}Cl_6]^{2-}$ and $[Pt^{37}Cl_6]^{2-}$, for the $[Pt^{35}Cl_n{}^{37}Cl_{5-n}(H_2{}^{16}O)]^-$ (n = 0−5), *cis*-$Pt^{35}Cl_n{}^{37}Cl_{(4-n)}(H_2{}^{16}O)_2$ (n = 0−4), and *fac*-$[Pt^{35}Cl_n{}^{37}Cl_{(3-n)}(H_2{}^{16}O)_3]^+$ (n = 0−3) isotopologues and isotopomers. The ^{195}Pt NMR chemical shifts computed for these species reproduce the order of magnitude of the observed effect reasonably well, up to ca. 1 ppm. In most cases, general trends are also captured qualitatively, thus providing the first theoretical basis for the origin of subtle isotope shifts in ^{195}Pt NMR spectra. The most important conclusion of our study is that the changes in bond distances necessary to rationalize these isotope shifts are but on the femtometer scale.

The quantitative accuracy of our protocol leaves much to be desired, however. From evidence for subtle solvation effects on the relative strengths of Pt−OH_2 vs Pt−Cl bonds, it appears that proper inclusion of solvation is of the essence. Unfortunately, neither simple polarizable continuum models nor small, microsolvated complexes lead to improved isotope shifts for the series investigated. Further studies are underway to explore the applicability and limitations of our protocol for the computation of subtle isotope shifts.

■ ASSOCIATED CONTENT

Supporting Information

Additional graphical and tabular material. This material is available free of charge via the Internet at http://pubs.acs.org.

■ AUTHOR INFORMATION

Corresponding Author

*Fax: (+44)(0)1334 463808 (M.B.); (+27)(0) 808 3342 (K.R.K.). E-mail: buehl@st-andrews.ac.uk (M.B.); krk@sun.ac.za (K.R.K.).

Notes

The authors declare no competing financial interest.

■ ACKNOWLEDGMENTS

This work was supported by the School of Chemistry in St. Andrews and by EaStChem via the EaStChem Research Computing facility and a local Opteron PC cluster maintained by Dr. H. Früchtl. We gratefully acknowledge financial support from Stellenbosch University (bursary to J.C.D. in terms of an exchange agreement between St. Andrews and Stellenbosch University) as well as Angloplatinum Ltd.

■ REFERENCES

(1) (a) Priqueler, J. R. L.; Butler, I. S.; Rochon, F. D. *Appl. Spectrosc. Rev.* **2006**, *41*, 185−226. (b) Still, B. M.; Kumar, P. G. A.; Aldrich-Wright, J. R.; Price, W. S. *Chem. Soc. Rev.* **2007**, *36*, 665−686.

(2) Ismail, I. M.; Kerrison, S. J. S.; Sadler, P. J. *J. Chem. Soc., Chem. Commun.* **1980**, 1175.

(3) Preetz, W.; Peters, G.; Bublitz, D. *Chem. Rev.* **1996**, *96*, 977.

(4) (a) Jameson, C. J.; Jameson, A. K. *J. Chem. Phys.* **1986**, *85*, 5484. (b) Jameson, C. J.; Jameson, A. K.; Oppusunggu, D. *J. Chem. Phys.* **1986**, *85*, 5480. (c) Jameson, C. J.; Rehder, D.; Hoch, M. *J. Am. Chem. Soc.* **1987**, *109*, 2589.

(5) Gerber, W. J.; Murray, P.; Koch, K. R. *Dalton Trans.* **2008**, 4113.

(6) Bühl, M. *Annu. Rep. NMR Spectrosc.* **2008**, *64*, 77−126.

(7) (a) Autschbach, J.; Le Guennic, B. *Chem.−Eur. J.* **2004**, *10*, 2581−2589. (b) Sterzel, M.; Autschbach, J. *Inorg. Chem.* **2006**, *45*, 3316−3324. (c) Autschbach, J.; Zheng, S. H. *Magn. Reson. Chem.* **2008**, *46*, S45−S55. (d) Krykunov, M.; Ziegler, T.; van Lenthe, E. *J. Phys. Chem. A* **2009**, *113*, 11495−11500. (e) Koch, K. R.; Burger, M. R.; Kramer, J.; Westra, A. N. *Dalton Trans.* **2006**, 3277−3284.

(8) (a) Grigoleit, S.; Bühl, M. *J. Chem. Theory Comput.* **2005**, *1*, 181−193. (b) Bühl, M.; Grigoleit, S.; Kabrede, H.; Mauschick, F. T. *Chem.−Eur. J.* **2006**, *12*, 477−488.

(9) (a) Perdew, J. P.; Burke, K.; Ernzerhof, M. *Phys. Rev. Lett.* **1996**, *77*, 3865−3868. (b) Adamo, C.; Barone, V. *J. Chem. Phys.* **1999**, *110*, 6158−6170.

(10) Dolg, M.; Wedig, U.; Stoll, H.; Preuss, H. *J. Chem. Phys.* **1987**, *86*, 866−872.

(11) (a) Hehre, W. J.; Ditchfield, R.; Pople, J. A. *J. Chem. Phys.* **1972**, *56*, 2257−2261. (b) Hariharan, P. C.; Pople, J. A. *Theor. Chim. Acta* **1973**, *28*, 213−222.

(12) Bühl, M.; Reimann, C.; Pantazis, D. A.; Bredow, T.; Neese, F. *J. Chem. Theory Comput.* **2008**, *4*, 1449−1459.

(13) Vosko, S. H.; Wilk, L.; Nusair, M. *Can. J. Phys.* **1980**, *58*, 1200−1211 Functional III of that paper used.

(14) (a) Becke, A. D. *J. Chem. Phys.* **1993**, *98*, 5648−5642. (b) Lee, C.; Yang, W.; Parr, R. G. *Phys. Rev. B* **1988**, *37*, 785−789.

(15) Perdew, J. P. In *Electronic Strucure of Solids*; Ziesche, P., Eischrig, H., Eds.; Akademie Verlag: Berlin, 1991. (b) Perdew, J. P.; Wang, Y. *Phys. Rev. B* **1992**, *45*, 13244−13249.

(16) See: (a) Barone, V.; Cossi, M. *J. Phys. Chem. A* **1998**, *102*, 1995−2001. (b) Cossi, M.; Rega, N.; Scalmani, G.; Barone, V. *J. Comput. Chem.* **2003**, *24*, 669−681 and references therein.

(17) (a) Ruud, K.; Åstrand, P.-O.; Taylor, P. R. *J. Chem. Phys.* **2000**, *112*, 2668−2683. (b) Ruud, K.; Åstrand, P.-O.; Taylor, P. R. *J. Am. Chem. Soc.* **2001**, *123*, 4826−4833. (c) Ruden, T.; Lutnæss, O. B.; Helgaker, T. *J. Chem. Phys.* **2003**, *118*, 9572−9581.

(18) (a) Barone, V. *J. Chem. Phys.* **2004**, *120*, 3059−3065. (b) Barone, V. *J. Chem. Phys.* **2005**, *122*, 014108.

(19) Frisch, M. J.; Trucks, G. W.; Schlegel, H. B.; Scuseria, G. E.; Robb, M. A.; Cheeseman, J. R.; Scalmani, G.; Barone, V.; Mennucci, B.; Petersson, G. A.; Nakatsuji, H.; Caricato, M.; Li, X.; Hratchian, H. P.; Izmaylov, A. F.; Bloino, J.; Zheng, G.; Sonnenberg, J. L.; Hada, M.; Ehara, M.; Toyota, K.; Fukuda, R.; Hasegawa, J.; Ishida, M.; Nakajima, T.; Honda, Y.; Kitao, O.; Nakai, H.; Vreven, T.; Montgomery, J. A., Jr.; Peralta, J. E.; Ogliaro, F.; Bearpark, M.; Heyd, J. J.; Brothers, E.; Kudin, K. N.; Staroverov, V. N.; Kobayashi, R.; Normand, J.; Raghavachari, K.; Rendell, A.; Burant, J. C.; Iyengar, S. S.; Tomasi, J.; Cossi, M.; Rega, N.; Millam, J. M.; Klene, M.; Knox, J. E.; Cross, J. B.; Bakken, V.; Adamo, C.; Jaramillo, J.; Gomperts, R.; Stratmann, R.

E.; Yazyev, O.; Austin, A. J.; Cammi, R.; Pomelli, C.; Ochterski, J. W.; Martin, R. L.; Morokuma, K.; Zakrzewski, V. G.; Voth, G. A.; Salvador, P.; Dannenberg, J. J.; Dapprich, S.; Daniels, A. D.; Farkas, Ö.; Foresman, J. B.; Ortiz, J. V.; Cioslowski, J.; Fox, D. J. *Gaussian 09*, revision A.1; Gaussian, Inc.: Wallingford, CT, 2009.

(20) Test calculations using the full QZ4P basis on all atoms indicated only minor differences from the locally dense QZ4P/TZP basis; specifically, the isotope shifts between isotopomers A and I of complex **2** (cf. Figure 2) differed by just 0.06 ppm (6%) between the two basis sets.

(21) Baerends, E. J.; Ziegler, T.; Autschbach, J.; Bashford, D.; A. Bérces, Bickelhaupt, F.M.; Bo, C.; Boerrigter, P. M.; Cavallo, L.; Chong, D. P.; Deng, L.; Dickson, R. M.; Ellis, D. E.; van Faassen, M.; Fan, L.; Fischer, T. H.; Fonseca Guerra, C.; Ghysels, A.; Giammona, A.; van Gisbergen, S. J. A.; Götz, A. W.; Groeneveld, J. A.; Gritsenko, O. V.; Grüning, M.; Gusarov, S.; Harris, F. E.; van den Hoek, P.; Jacob, C. R.; Jacobsen, H.; Jensen, L.; Kaminski, J. W.; van Kessel, G.; Kootstra, F.; Kovalenko, A.; Krykunov, M. V.; van Lenthe, E.; McCormack, D. A.; Michalak, A.; Mitoraj, M.; Neugebauer, J.; Nicu, V. P.; Noodleman, L.; Osinga, V. P.; Patchkovskii, S.; Philipsen, P. H. T.; Post, D.; Pye, C. C.; Ravenek, W.; Rodríguez, J. I.; Ros, P.; Schipper, P. R. T.; Schreckenbach, G.; Seldenthuis, J. S.; Seth, M.; Snijders, J. G.; Solà, M.; Swart, M.; Swerhone, D.; te Velde, G.; Vernooijs, P.; Versluis, L.; Visscher, L.; Visser, O.; Wang, F.; Wesolowski, T. A.; van Wezenbeek, E. M.; Wiesenekker, G.; Wolff, S. K.; Woo, T. K.; Yakovlev, A. L.. *ADF2010*; SCM, Theoretical Chemistry, Vrije Universiteit: Amsterdam, The Netherlands; see http://www.scm.com.

(22) Fowe, E. P.; Belser, P.; Daul, C.; Chermette, H. *Phys. Chem. Chem. Phys.* **2005**, *7*, 1732−1738.

(23) Although the minimum turned out to possess C_2 symmetry, the calculations were done without imposing this. The differences in results for formally equivalent bonds can thus be a further probe for numerical stability.

(24) Bühl, M.; Imhof, P.; Repisky, M. *ChemPhysChem* **2004**, *5*, 414−418.

(25) Grigoleit, S.; Bühl, M. *Chem.−Eur. J.* **2004**, *10*, 5541−5552.

(26) See, e.g., Martinez, J. M.; Pappalardo, R. R.; Sanchez Marcos, E.; Mennucci, B.; Tomasi, J. *J. Phys. Chem. B* **2002**, *106*, 1118−1123.

(27) For a review, see: Bühl, M.; Wipff, G. *ChemPhysChem* **2011**, *12*, 3095−3105, DOI: 10.1002/cphc.201100458.

(28) Bühl, M.; Sieffert, N.; Chaumont, A.; Wipff, G. *Inorg. Chem.* **2011**, *50*, 299−308.

(29) E.g. Beret, E. C.; Martinez, J. M.; Pappalardo, R. R.; Marcos, E. S.; Doltsinis, N. L.; Marx, D *J. Chem. Theory Comput.* **2008**, *4*, 2108−2121.

(30) See, e.g., (a) Truflandier, L. A.; Autschbach, J. *J. Am. Chem. Soc.* **2010**, *132*, 3472−3483. (b) Truflandier, L. A.; Sutter, K.; Autschbach, J. *Inorg. Chem.* **2011**, *50*, 1723−1732.

(31) We note that even though MD simulations depend on the atomic masses, it seems all but impossible at this time to converge the simulations to such a numerical precision that would allow extraction of classical thermal isotope effects of the small magnitude required for our purposes.

(32) Arcisauskaite, V.; Melo, J. I.; Hemmingsen, L.; Sauer, S. P. A. *J. Chem. Phys.* **2011**, *135*, 044306.

(33) For lighter nuclei see, e.g., ref 17 and Wigglesworth, R. D.; Raynes, W. T.; Kirpekar, S.; Oddershede, J.; Sauer, S. P. A. *J. Chem. Phys.* **2000**, *112*, 736−746.

(34) For typical 3d-metal complexes, this effect on absolute shieldings is ca. 1−2 ppm for chloride complexes (somewhat larger for carbonyls); cf. σ_0 vs σ_{eff} values in ref 25.